Solvation and Thermalization of Electrons Generated by above-the-Gap (12.4 eV) Two-Photon Ionization of Liquid H_2O and D_2O

Rui Lian, Robert A. Crowell,* and Ilya A. Shkrob

Chemistry Division, Argonne National Laboratory, 9700 S. Cass Avenue, Argonne, Illinois 60439

Received: September 24, 2004; In Final Form: December 9, 2004

Temporal evolution of transient absorption (TA) spectra of electrons generated by above-the-gap (12.4 eV total energy) two-photon ionization of liquid H_2O and D_2O has been studied on femto- and picosecond time scales. The spectra were obtained at intervals of 50 nm between 0.5 and 1.7 μm. Two distinct regimes of the spectral evolution were observed: $t < 1$ ps and $t > 1$ ps. In both of these regimes, the spectral profile changes considerably with the delay time of the probe pulse. The "continuous blue shift" and the "temperature jump" models, in which the spectral profile does not change as it progressively shifts, as a whole, to the blue, are not supported by our data. Furthermore, no p-state electron, postulated by several authors to be a short-lived intermediate of the photoionization process, was observed by the end of the 300 fs, 200 nm pump pulse. For $t < 1$ ps, two new TA features (the 1.15 μm peak and 1.4 μm shoulder) were observed for the electron in the spectral region where O−H overtones appear in the spectra of light water. These two features were not observed for the electron in D_2O. The 1.4 μm peak observed in D_2O may be the isotope-shift analogue of the 1.15 μm feature in H_2O. Vibronic coupling to the modes of water molecules lining the solvation cavity is a possible origin of these features. On the sub-picosecond time scale, the absorption band of solvated electron progressively shifts to the blue. At later delay times ($t > 1$ ps), the position of the band maximum is "locked", but the spectral profile continues to change by narrowing on the red side and broadening on the blue side; the oscillator strength is constant within 10%. The time constant of this narrowing is ca. 0.56 ps for H_2O and 0.64 ps for D_2O. Vibrational relaxation and time-dependent decrease in the size and sphericity of the solvation cavity are suggested as possible causes for the observed spectral transformations in both of these regimes.

1. Introduction

Although ultrafast dynamics of the excess electron in liquid water have been extensively studied over the past 2 decades, many questions concerning the mechanism of localization, solvation, and thermalization of this electron still remain. Using femtosecond pump−probe transient absorbance (TA) laser spectroscopy, short-lived precursors (which in the following will be collectively called "presolvated" electrons) of the hydrated, thermalized electron have been observed on sub-picosecond to picosecond time scales.[1−17] Common means of generating these presolvated electrons include multiphoton ionization of neat water,[1−6,13−16] photoionization of molecular solutes and electron photodetachment from aqueous anions,[2,16,17] and photoexcitation of hydrated electrons.[7−12] The initial studies[1−5] were limited to the observation of the TA signal for a few strategically chosen probe wavelengths in the visible and near-infrared (>1 μm). Recently, the observation range has been expanded into the ultraviolet (down to 200 nm)[14] and mid-infrared (out to 5 μm).[16] The latter studies seem to suggest the existence of two infrared (IR) absorbing precursors of the hydrated electron, e_{aq}^-. One of these species has a broad absorption band centered at 1.6 μm (suggesting a localized state in a shallow trap),[16] while another species has a featureless spectrum that resembles that of a free (extended state) conduction band electron in semiconductors or a long-lived, IR-absorbing electron in low-temperature ice.[19−21] While the existence of the short-lived IR-absorbing species has been hinted at by the pioneering studies of Migus et al.[1] and spectral decomposition analyses of Gauduel and co-workers,[3−5] subsequent work on electron solvation in photoionization of water favored the so-called "continuous shift" model[6,13,17,22−25] in which the existence of these IR-absorbing species (such as shallow-trap "wet" electrons)[6,11,16] is not strictly required. In the latter model, the absorption profile $S(E,t)$ of the presolvated electron as a function of photon energy E is postulated to shift, as a whole, to the blue during the solvation, without changing its shape.

In a more recent variant of this model suggested by Madsen et al.[15] (which is referred to in the following as the "temperature jump" model), the thermalization is regarded as "cooling" of water around the solvation cavity in which the absorption spectrum of the electron at any time during the thermalization process is identical to the spectrum of hydrated electron in the state of equilibrium with the solvent at some higher temperature. In this model, the electron thermalization is viewed as a succession of quasi-equilibrium states that are fully characterized by the time evolution of the local temperature. This model, like the original "continuous shift" model is phenomenological: no explanation is given, on theoretical grounds, as to why such a picture of the electron solvation might be correct. The width of the spectrum for e_{aq}^- depends weakly on the water temperature, whereas the position of the absorption maximum is strongly temperature dependent.[26] From the standpoint of data analysis, the temperature jump model of Madsen et al.[15] is identical to the continuous shift model. The same applies to the "cavity contraction" model of Unterreiner and co-workers[13] (see section

* To whom correspondence should be addressed. Telephone: 630-252-8089. Fax: 630-2524993. E-mail: rob_crowell@anl.gov.

10.1021/jp045657b CCC: $30.25
Published on Web 02/04/2005

4.2). Despite their appealing simplicity, both the continuous shift model and its variants[13,15] are inadequately supported.

First, in many ultrafast studies, the TA spectra were too sparsely sampled: the TA kinetics were obtained for just a few wavelengths of the probe light.[3−5,13,17] This sparse sampling makes it impossible to verify the central tenet of the continuous shift model, viz., the constancy of the spectral profile during the thermalization process. Due to the large spectral bandwidth of short light pulses, TA experiments which use very short probe pulses are inherently less sensitive to the fine details of spectral evolution. Since improving the temporal resolution has been the main thrust in the electron solvation studies, the test of the continuous shift model was not given a priority. Typically, the constancy of the spectral profile was *postulated* rather than observed: For a given delay time t of the probe pulse, the TA spectrum was fit by a constant-profile template using least-squares optimization. As a result, the experimental spectrum is characterized by a single parameter, $E_{max}(t)$, the photon energy corresponding to the absorption maximum. Naturally, this procedure tells little about the robustness of the template used to fit the experimental spectrum since any deviation from the prescribed shape is regarded as statistical deviation. Worse, the exact location of the maximum strongly depends on the template used to fit the data, inasmuch as the electron spectra are flat at the top, broad, and featureless, so that $E_{max}(t)$ is determined, implicitly or explicitly, by the extrapolation of the data in the spectral wings toward the center, where the TA signal is maximum. If the profile of these TA spectra were time-dependent (as suggested by our results), this approach would yield incorrect results.

Second, the TA studies in which the spectral sampling was denser (at least 10−15 wavelengths of the probe light across the spectrum, so that the time-dependent shape of the spectrum can be studied) *did not* fully support the continuous shift model. For example, the studies by Gauduel and co-workers[3−5] and Pepin et al.[6] on electron dynamics in H_2O and D_2O, respectively, suggested that the continuous shift alone cannot account for the observed spectral evolution. In the latter study, an additional long-lived (>2 ps) species with a spectral band centered at 1.1−1.3 μm was postulated to explain the evolution of the TA spectrum for $\lambda > 0.9$ μm. Subsequent pump−probe studies failed to verify the existence of such a long-lived species. Pepin et al.[6] conceded that more TA studies with dense sampling of the TA kinetics across a wider spectral region and better quality kinetic data would be needed to characterize the spectral evolution and establish the validity of the continuous shift model. The present study implements such a program.

Third, it is now understood that the electrons generated in different photoprocesses have different thermalization[9] and geminate recombination[9,27−29] dynamics. Specifically, in photoionization of neat water, different excitation mechanisms operate for photons of different energy.[27−29] Two- or three-photon excitation at the lower photon energy (so that the total excitation energy < 9 eV) produces electrons that are, on average, just 0.9−1 nm away from their parent hole, whereas, at higher total photon energy (>11 eV), the photoelectrons are at least 2−3 nm away.[27,28] It is believed that, for high-energy photoexcitation, the electrons are ejected directly into the conduction band of the solvent; at lower energy, the photoionization involves concerted proton and electron transfers, perhaps to preexisting traps.[30−32] In the intermediate regime, autoionization of water is thought to compete with these two photoprocesses.[28] The studies with the densest spectral sampling, which allowed determination of the evolution of the spectral profile,[5,6] were carried out in these low-energy and intermediate regimes. Due to the short separation distances between the geminate partners, some electrons decayed during the fist few picoseconds when their solvation and thermalization had occurred.[6] This decay had to be taken into account, by extrapolation of the picosecond dynamics to short delay times. Such a procedure implies that the presolvated electron follows the same recombination dynamics as fully hydrated and thermalized electron, which may not be correct. For example, recent simulations of spectral evolution for electrons generated by photodetachment from aqueous iodide (carried out using the continuous shift model) by Vilchiz et al.[17] suggested significant recombination of the short-lived presolvated species.

In the present study, femto- and picosecond TA kinetics were obtained for the electron generated by a high-energy ionization photoprocess (12.4 eV total energy); in this regime, geminate recombination on the picosecond time scale is unimportant.[29] Short (300 fs full width at half-maximum (fwhm)) 200 nm laser pulses were used to photoionize room-temperature H_2O and D_2O, by promoting the electron into the conduction band, via biphotonic excitation.[29] Our results suggest that the continuous shift model does not account for the spectral evolution occurring during electron solvation/thermalization in light and heavy water.

We forewarn the reader that no specific physical or microscopic model that accounts for these observations is given in this paper. Many models of electron solvation and relaxation, at all levels of theory, have been suggested. Given the limited success that these theories met in the explanation of experimental observations, offering yet another such model seems injudicious. Rather, we focus on the spectral features themselves and what can be glimpsed from these features without the benefit of theoretical insight. Such an insight is certainly needed, but it is beyond the scope of this study.

Hereafter, the index "S" (e.g., Figure 1S) indicates that the material is placed in the Supporting Information available electronically from the journal. Appendices A and B are also placed therein.

2. Experimental Section

2.1. Materials. Deionized water with conductivity < 2 nS/cm was used in all experiments with H_2O. An N_2-saturated 1 L sample was circulated using a gear pump through a jet nozzle; the conductivity of this circulated water was < 1 μS/cm. A 500 mL sample of heavy water (99 at. %, Aldrich) was used in all experiments with D_2O. No change in the kinetics was observed after extensive photolysis of this sample. The details of the flow system are given elsewhere.[33]

2.2. Ultrafast Laser Spectroscopy. The pico- and femtosecond TA measurements were carried out using a 1 kHz Ti:sapphire setup, details of which are given in refs 29 and 33. This setup provided 60 fs fwhm, 3 mJ light pulses centered at 800 nm. One part of the beam was used to generate probe pulses, while the other part was used to generate the 200 nm (fourth harmonic) pump pulses. Up to 20 μJ of the 200 nm light was produced this way (300−350 fs fwhm pulse). The pump and probe beams were perpendicularly polarized and overlapped at the surface of a 90 μm thick high-speed water jet at 5°. No change of the TA kinetics with the polarization of the probe light was observed.

A white light supercontinuum was generated by focusing the 800 nm fundamental on a 1 mm thick sapphire disk; the probe light was selected using a set of 10 nm fwhm interference filters (Corion). For two wavelengths, 1.6 and 1.7 μm (used in the studies of electron in D_2O), the intensity of the probe light was

weak and 30 nm fwhm band-pass filters were used instead. Appropriate glass cutoff filters were used to block stray 200, 400, and 800 nm light. For measurements in the near-infrared, 0° dielectric mirrors for 800 nm light were inserted in the path of the probe beam to reduce the leakage of the fundamental. Fast Si photodiodes (FND100Q from EG&G) were used for detection of the $\lambda < 1.1$ μm light; fast Ge photodiodes (GMP566 from GPD Optoelectronics Corp.) were used for detection of $\lambda > 1.1$ μm. The vertical bars in the figures represent 95% confidence limits for each data point.

To study the thermalization dynamics of the electron, the delay time was increased in steps of 50 fs to 5−7 ps and steps of 300 fs to 25 ps. The kinetic origin (i.e., zero delay time t) and the $1/e$ width τ_p of the 200 nm excitation pulse convoluted with the probe pulse were determined by following the TA signal from a 1.4 μm thick amorphous Si:H alloy (8 at. % H) film on a suprasil substrate.[34] The instantaneous increase in the TA signal near the kinetic origin is from the generation of free electron carriers in the Si:H sample;[35] the slower decay kinetics are due to the thermalization, trapping, and recombination of these photocarriers.[34,35] Deconvolution of these TA signals (represented as a Gaussian pulse convoluted with biexponential decay to a plateau) gives the "pulse width" (τ_p, characteristic of the response function of the setup). Due to the considerable chirp in the 200 nm pump pulse (introduced by harmonic generating BBO crystals and focusing optics), τ_p was 190−290 fs, depending on the optimization of the compressor and the probe wavelength. The latter dependence is due to the wavelength-dependent chirp in the white light continuum and group velocity mismatch (GVM) in the water sample (traceable to the difference in the speed of light for the pump and probe pulses). The variation in the pulse width and the resulting uncertainty in the time origin made it difficult to obtain good-quality electron spectra for $t < 500$ fs. For $\lambda < 700$ nm, the TA traces exhibit a sharp "spike" at the time origin (see Figure 1a in section 3) whose time profile follows the photoresponse function of the detection system. This TA signal in the visible has been observed by other workers[6,13,17] and originates from nonlinear absorbance of the excitation and probe light in the sample. It can be used to juxtapose the corresponding kinetics in time without a reference to the Si:H sample. Since the photoexcitation wavelength of 200 nm is right at the onset of one-photon water ionization (the quantum yield of this ionization is ca. 1.6×10^{-2} at 193 nm),[36] this artifact may be present even when red and near-infrared light is used to probe the electron dynamics (section 4.2).

The kinetic traces given below were obtained using a 1−5 μJ pump pulse focused, using a thin MgF_2 lens, to a round spot of 300 μm fwhm; the probe beam was typically 50−60 μm fwhm. The typical TA signal (ΔOD_λ, where λ is the wavelength of the probe light in nanometers) at the maximum was 10−50 mOD. The TA signal $\Delta OD_{800}(t)$ from hydrated electron obtained at the delay time $t = 10$ ps plotted as a function of 200 nm power scaled as the square of the pulse energy, indicating biphotonic ionization.[29]

2.3. Reconstruction of the Electron Spectrum. Time-dependent TA spectra $S(\lambda,t)$ given below were obtained from the TA kinetics using the following approach:[13,17] The kinetics (obtained independently for each probe wavelength λ) were normalized by the average of the TA signal at $t = 5-8$ ps. At this delay time, the $\Delta OD_\lambda(t)$ kinetics reach a plateau: the thermalization phase is complete (see section 3), yet the electron decay due to geminate recombination is still negligible.[29] These normalized kinetics were then weighted by the spectrum $S(\lambda)$ of the thermalized (hydrated electron) to obtain the time-dependent spectrum $S(\lambda,t)$ of the presolvated electron:

$$S(\lambda,t) = S(\lambda)\ \Delta OD_\lambda(t)/\Delta OD_\lambda(t{=}5-8\text{ps}) \qquad (1)$$

For $\lambda > 1$ μm, where e_{aq}^- absorbs poorly, the use of this procedure requires more comment (see Appendix A).

First, since the TA signal from the hydrated electron at $t > 5$ ps becomes very small relative to the "spike" from the presolvated electron (Figures 1−3), even a small error of a few percent in the scaling factor $S(\lambda)$ in eq 1 has a large effect on the extrapolated $S(\lambda,t)$ signal at short delay time. Thus, a high-quality *near-infrared* spectrum of e_{aq}^- in light and heavy water was needed. To this end, a separate flash photolysis study was carried out to obtain a spectrum of e_{aq}^- in H_2O ($\lambda = 0.4-1.4$ μm) and D_2O ($\lambda = 0.4-1.7$ μm) (see Appendices A.1 and A.2).

Second, one should be aware that the weak, long-lived TA signal observed at $t > 5$ ps might not be related to e_{aq}^- since the solvent itself weakly absorbs in the near-infrared (where overtones of the O−H stretch appear). Specifically, a long-lived thermal signal from laser-heated water could change the transmittance of the probe light, e.g., through a change of the refractive index. To address such a possibility, 1 M $HClO_4$ was added to H_2O (hydronium ion scavenges e_{aq}^- with a rate constant of 2.3×10^{10} M^{-1} s^{-1}).[27] This scavenging removed most of the TA signal in the first 300 ps. By comparing the long-term kinetic traces obtained at different wavelengths, we were able to demonstrate that at least 90−95% of the TA signal at 1.1−1.3 μm was from e_{aq}^- (Figure 4S in the Supporting Information). However, for $\lambda > 1.3$ μm, the long-lived TA signal was too weak to obtain good-quality decay kinetics on the sub-nanosecond time scale. Thus, we cannot presently confirm that *all* of the long-lived TA signal in the near-infrared is due to the absorbance from e_{aq}^- . This uncertainty introduces ambiguity in the reconstruction of the near-infrared spectra using eq 1. We will return to this point in section 4.2.

Third, it is nearly impossible to retain the same characteristics of the probe light (such as its pulse width, chirp, and GVM) across the entire spectral region of interest. For this reason, obtaining reliable TA spectra $S(\lambda,t)$ using eq 1 for delay times $t < 500$ fs is impossible without (i) making specific assumptions about these pulse characteristics and (ii) using ad hoc kinetic schemes for spectrum modeling (as done, for example, in refs 5, 16, 17, 22, and 23). Since these kinetic schemes are not unique, the robustness of such analyses is impossible to estimate. Our approach is to analyze the data with as few assumptions as possible, and for this reason we focus on the evolution of the TA spectra that occurs between 0.5 and 3 ps after the 12.4 eV photoionization.

3. Results

Typical TA kinetics observed for presolvated electron following two 200 nm photon ionization of light water are shown in Figures 1−3. The complete set of digitized kinetic traces is given in the Supporting Information (see Appendix B for instructions). Most of the trends observed in these kinetic traces have already been seen by others. For $\lambda > 0.8$ μm, the TA signal rapidly increases within the duration of the 200 nm pulse and then slowly decreases to a plateau (Figures 1b, 2b, and 3a). The ratio of the maximum TA signal to the signal attained at $t = 5$ ps increases with increasing probe wavelength λ (e.g., Figure 3). For D_2O, this ratio increases from ca. 5:1 at 1.1 μm to ca. 10:1 at 1.25 μm to ca. 30:1 at 1.4 μm to ca. 50:1 at 1.6

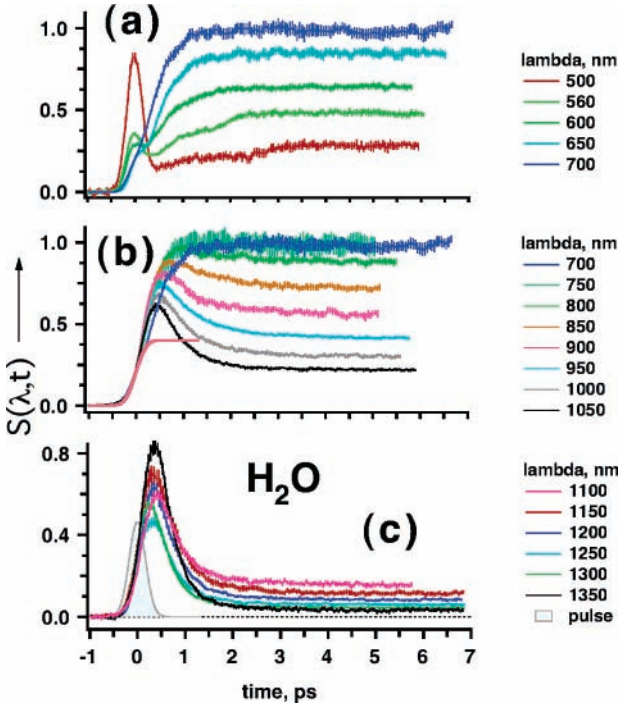

Figure 1. Family of kinetic traces $S(\lambda,t)$ (section 2 and eq 1) for electron generated by bi-200-nm photonic ionization of the room-temperature light water. The magnitude of the hydrated electron spectrum at the maximum is taken as unity. The probe wavelength λ (500−1350 nm) is given in the color scales to the right of the plots. The vertical bars are 95% confidence limits. The "spike" near the kinetic origin in a is from nonlinear absorbance due to simultaneous absorption of 200 nm and probe photons. The sigmoid curve in b is the integral of the response function of the system (which is shown by a shaded curve in c).

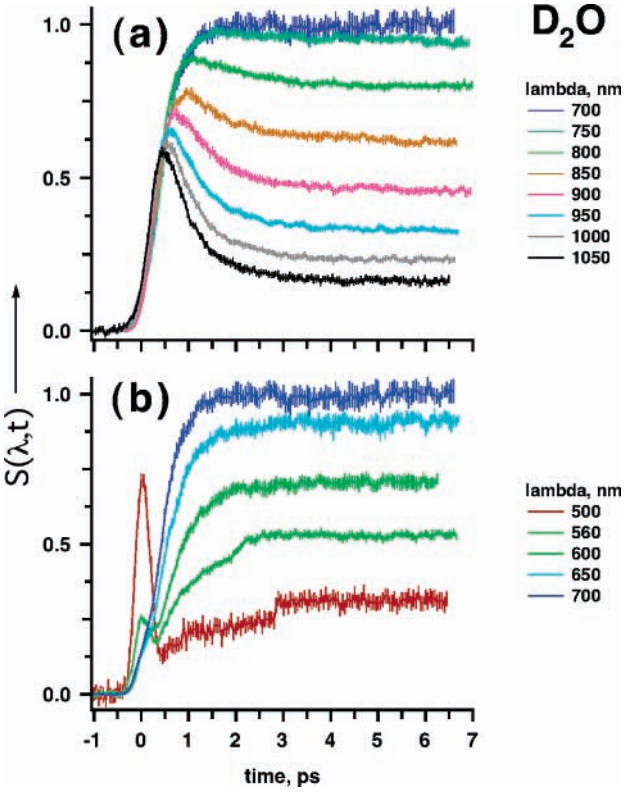

Figure 2. Same as Figure 1, for heavy water. Only 500−1050 nm data are shown.

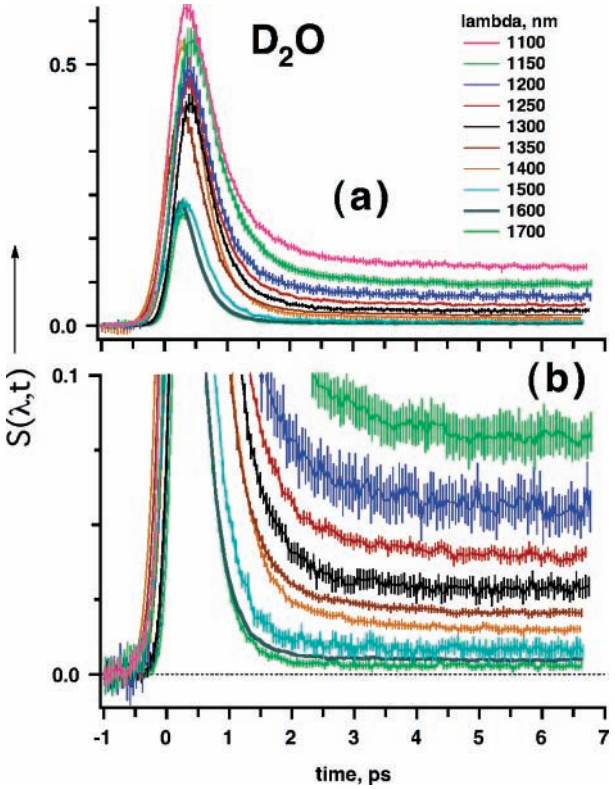

Figure 3. Same as Figure 1, for heavy water. Only 1100−1700 nm data are shown. In b, the vertical scale is expanded to illustrate the nonzero plateau attained at $t > 3$ ps.

μm. As the plateau absorbance becomes smaller (with respect to the maximum TA signal) with increasing λ, the decay kinetics also become progressively faster (e.g., compare the 0.85 and 1.5 μm traces in Figures 2a and 3a, respectively). In the visible ($\lambda = 0.5-0.75$ μm), the increase in the TA signal is relatively slow (which occurs over the first 2 ps after the ionization, Figures 1a and 2a) and the changes in the kinetic profiles with the wavelength are less pronounced than for $\lambda > 0.8$ μm.

Qualitatively, these trends can be accounted for by a progressive blue shift of the absorption band of the ground-state electron in the course of its solvation and thermalization.[6,13,17,22−24] Initially, the electron localizes in a large cavity and interacts with the H−O dipoles of water molecules weakly, absorbing in the near-infrared. At later delay times, the cavity contracts, the interaction becomes stronger, and the absorption band shifts to the visible so that the TA signal in the near-infrared rapidly decays (since e_{aq}^- is a weak absorber in this region) and the TA signal in the visible increases (since e_{aq}^- absorbs strongly in the red). The ratio of the maximum TA signal to the plateau value increases with the wavelength λ because the absorptivity of e_{aq}^- rapidly decreases in the same direction. The change in the TA signal is faster where a small change in the wavelength results in a large change in the TA signal, as occurs in the near-infrared. In this general outline of the spectral evolution, our study fully concurs with the previous results. However, these features per se do not imply that the profile of the TA spectrum remains constant during the spectral shift.

To characterize the spectral evolution of photoelectron during its solvation, the method outlined in section 2 and Appendix A has been used. For reasons explained therein, the use of this method is justified only for relatively long delay times, $t > 0.5$ ps. The spectra $S(\lambda,t)$ obtained using eq 1 were linearly interpolated in the time domain and then integrated between the delay times t_1 and $t_2 = t_1 + \Delta t$, to obtain the average

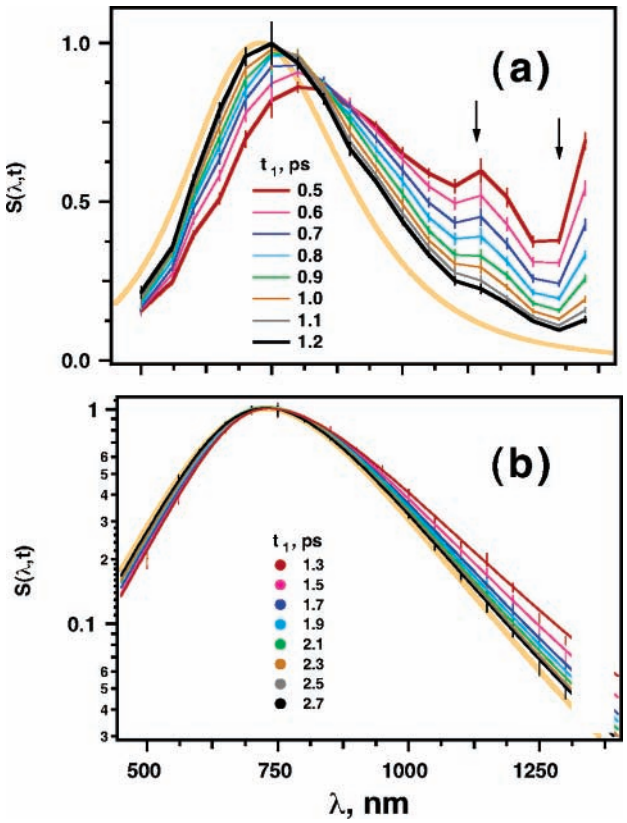

Figure 4. TA spectra $S(\lambda,t)$ for electron in light water at different intervals (t_1, $t_1 + \Delta t$) of delay time. The delay times t_1 are given in the plots. For a, $\Delta t = 100$ fs; for b, 200 fs. The maximum TA signal from the hydrated electron $S(\lambda) = S(\lambda,t=\infty)$ is taken as unity. The solid lines in b are Gaussian−Lorentzian functions obtained by least-squares fits, as explained in the text (note the logarithmic vertical scale). The vertical bars are 95% confidence limits. The bold solid line is the normalized spectrum ($S(\lambda)$) of fully thermalized hydrated electron. The vertical arrows indicate previously unobserved features in the near-infrared.

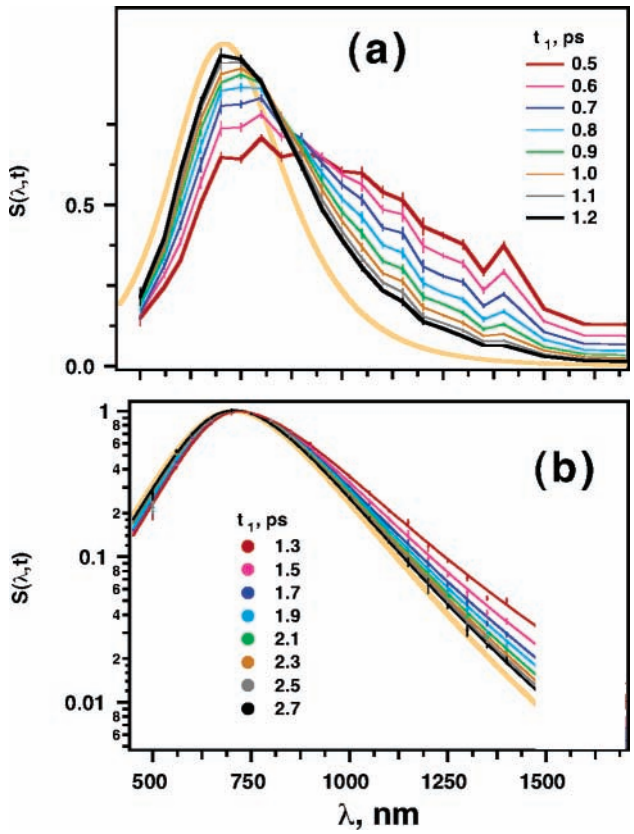

Figure 5. Same as Figure 4, for the electron in liquid D_2O.

spectrum for the corresponding (t_1,t_2) window. Figures 4a and 5a show several such spectra for electrons in light and heavy water, respectively, for delay times t_1 between 0.5 and 1.2 ps ($\Delta t = 100$ fs). Figures 4b and 5b show the spectral evolution at later delay times, from 1.3 to 2.7 ps ($\Delta t = 200$ fs). For comparison, the spectrum of a fully thermalized, solvated electron in H_2O and D_2O is indicated by a bold line. For $t > 1$ ps, the spectral evolution of the electron in light water (Figure 4b) is very similar to that in heavy water (Figure 5b). By contrast, on the sub-picosecond time scale, near-infrared spectra for electrons in H_2O (Figure 4a) look quite different from those in D_2O (Figure 5a).

On the short time scale (0.5−1.2 ps), the absorption band of the excess electron rapidly shifts to the blue. In Figure 6, the data of Figures 4a and 5a are plotted vs the photon energy, which emphasizes the systematic change in the shape of a spectral profile with delay time. As the band shifts, the spectrum narrows on both sides of the maximum. At $t = 1$−1.2 ps, the position E_{max} of the absorption maximum almost reaches its equilibrium value. For $t > 1.2$ ps, the band maximum is "locked" within 20 meV of its equilibrium value; however, the spectral evolution continues: on the red side, the absorption line becomes narrower, and on the blue side, it becomes broader (Figures 4b and 5b), by 50−100 meV. Thus, there are two distinct regimes in the spectral evolution of the electron: (i) the "fast (sub-picosecond) regime", in which the spectral features are dominated by the band shift to the blue and overall spectral narrowing and (ii) the "slow (> 1 ps) regime", in which the spectral evolution is dominated by small-scale spectral transformations occurring after E_{max} gets very close to its equilibrium value. In either one of these regimes, the "continuous blue shift" model provides a rather poor description of the spectral evolution observed.

4. Discussion

4.1. "Fast Regime" (0.5−1 ps). A curious feature of sub-picosecond TA spectra shown in Figures 4a and 5a is an "isosbestic point" at 0.85 μm observed in both light and heavy water.[5,6] On closer examination, this feature does not constitute a true isosbestic point since the TA spectra obtained at different delay times do not pass through any particular point of the e_{aq}^- spectrum within the confidence limits of our measurement. Some authors[5,6,23,24] view this feature as evidence for the existence of two or more types of presolvated electron coexisting at short delay time; the observed TA spectra are then "decomposed" into separate contributions from the electron states with either time-dependent[24] or time-independent[5] spectra.

The largest impetus for the two-state model of the electron solvation was given by the original studies of Migus et al.[1,3] who observed a broad, short-lived component at 0.9−1.3 μm for the electron in H_2O that decayed in the first picosecond after the multi-310-nm photon ionization. The overlap of this short-lived spectral component with the spectrum of the thermalized electron was thought to account for the "isosbestic point". Since the pump pulse in these pioneering studies was quite wide, this near-infrared feature was observed well within the duration of the photoexcitation pulse. Subsequent studies that used shorter pump pulses[13,17] failed to reproduce this feature. For the electron in D_2O, the progression of the TA spectra shown in Figure 5a has the same general appearance as that observed by Pépin et al.[6] following short-pulse multi-600-nm photon ionization of D_2O. Their spectra, in turn, are qualitatively similar to the recent

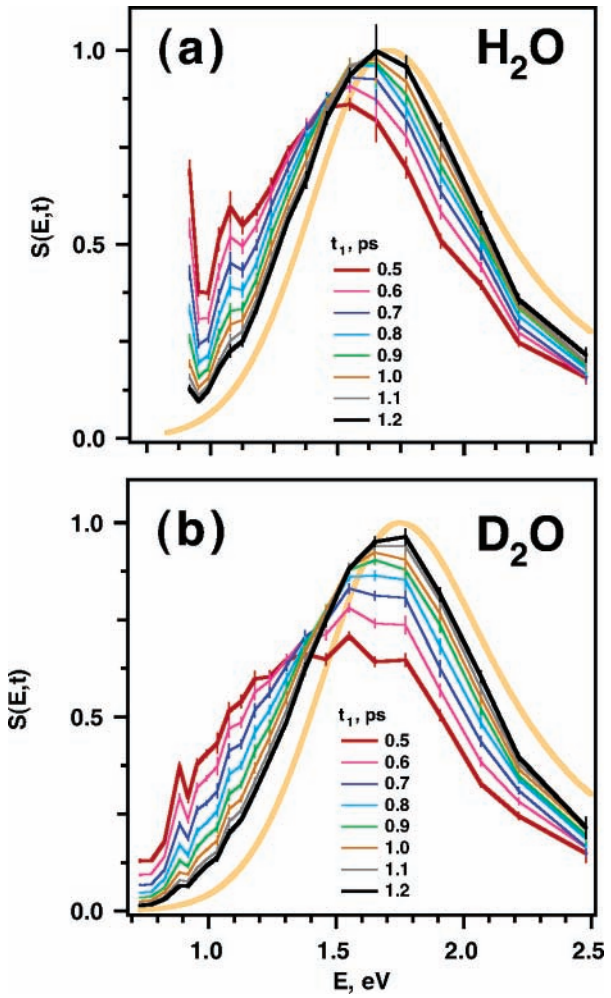

Figure 6. Spectral data of (a) Figure 4a and (b) Figure 5a replotted as a function of the photon energy E of the probe light, to illustrate inconstancy of the spectral profile during the shift.

data of Unterreiner and co-workers[13] and Vilchiz et al.[17] for the electron in H_2O who used short ultraviolet (UV) pulses generated by harmonic generation (on a Ti:sapphire laser system). Either the near-infrared feature observed by Migus et al.[1,3−5] is very short-lived (and, therefore, requires a relatively long excitation pulse to be observed against the background TA signal from the solvated electron) or, possibly, it is caused by nonlinear absorption of the probe light within the duration of the UV pulse (section 2).

The TA spectra obtained in this study within the duration of the excitation pulse also exhibit a diffuse absorption band in the near-infrared. In Figure 5S, the spectra $S(E,t)$ for the electron in D_2O are shown for the 0−250 and 250−500 fs time windows. The visible data were excluded from the plot due to the strong contribution from nonlinear absorbance (the "spike" in Figures 1a and 2b) that interferes with the measurement. While using the method of eq 1 at these short delay times is not justified, the resulting spectra resemble the ones reported by Migus et al.[1] and Gauduel et al.[3,5] In Figure 7, a near-infrared spectrum obtained in the point-to-point fashion within the last 10% of the duration of the 200 nm photoexcitation pulse is shown for the electron in D_2O. Once more, this spectrum is flat across the entire observation window; such a spectrum would be compatible with the existence of a short-lived (e_{IR}^-) species that strongly absorbs at $\lambda > 0.9$ μm. The transformation of this TA spectrum at the end of the 200 nm pulse to that shown in Figure 5a is very abrupt. Our data are insufficient to make a choice

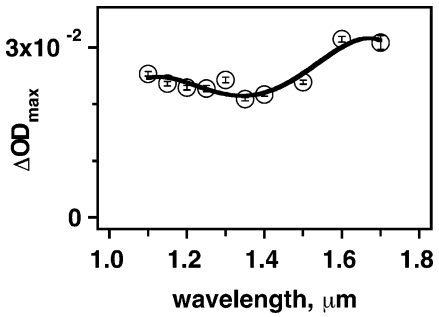

Figure 7. Open circles: TA signal for the electron in D_2O vs the wavelength λ of the probe light ($\lambda > 1.1$ μm). The delay time between the 200 nm pump and the probe pulses was fixed (this delay time corresponded to the last 10% of the pump pulse duration). The solid line is a guide to the eye.

between the two possibilities discussed above (nonlinear absorbance vs extremely short-lived species), and we leave the question open for further studies that use a shorter UV pulse.

Recently, Laenen et al.[16] obtained TA spectra in near- and mid-infrared after two 266 nm photon ionization of liquid H_2O and D_2O. In H_2O, a broad absorption band from an intermediate (which the authors identify as "wet" electron) with a lifetime of 0.54 ps was observed at 1.5−1.7 μm. In D_2O, this band is red-shifted to 2 μm (still, the absorbance at 1.2 μm is ca. 30% of the maximum). It is not clear from the published data how this feature evolves for $t > 0.5$ ps. Laenen et al.[16] give an estimate of 3×10^4 and 5×10^4 M^{-1} cm^{-1} for the molar absorptivity of the wet electron at 1.2 and 1.6 μm, respectively (in D_2O). Then, for these two probe wavelengths, a wet electron with a lifetime of 0.5−0.6 ps would yield a TA signal at $t =$ 0.5 ps which comprises 30−80% of the absorption signal from a fully hydrated electron (having molar absorptivity of 2×10^4 M^{-1} cm^{-1} at the band maximum).[26,37] No such TA signal was observed in our study.

Instead, two features indicated by arrows in Figure 4a were observed for the electron in light water: the 1.15 μm peak and the shoulder at 1.3−1.4 μm. Both of these features fully decay within the first picosecond after the photoionization, and their decay kinetics appear to be similar. Subtracting the 1.15 μm trace from the half-sum of the 1.1 and 1.2 μm traces, one obtains a kinetic profile that decays with a time constant of 0.2−0.3 ps, which is roughly the same time scale as that for the shift of the band maximum. The shoulder observed for $\lambda > 1.3$ μm might be the extension the 1.4−1.8 μm feature (from the putative wet electron) observed by Laenen et al.[16] It also looks similar to the 1.3 μm feature observed by Migus et al.[1] (a 0.24 ps lifetime was estimated for this feature therein).

We believe that these features are not artifacts of the spectral reconstruction procedure described in section 2 (which is also suggested by the reasonable agreement with the previous studies); however, such a possibility cannot be fully excluded. Since both of these features are observed in the region where liquid H_2O exhibits H−O vibration overtones, the concern is that the long-lived "absorbance" signal used for normalization of the TA kinetics is from the heat induced by the absorption of the UV light. The control experiments demonstrated that e_{aq}^- scavenging by 1 M acid removes >90−95% of the 1.0−1.3 μm signal; i.e., at most 5−10% of this long-lived TA signal could be from the thermal effect. This would be insufficient to account for the 1.15 μm feature which comprises ca. 20% of the TA signal at this wavelength. For the $\lambda > 1.3$ μm shoulder, such a test was difficult to conduct and we cannot discount the thermal effect entirely. It is, however, unlikely that the dynamics

of such an effect would closely follow the dynamics of the 1.15 μm feature. Importantly, the 1.4 μm feature observed in D_2O (Figure 5a) may be the isotope-shift analogue of the 1.15 μm feature in H_2O, provided that these two features originate from the O−D and O−H vibration overtones, as suggested in section 4.3. (The analogue of the 1.4 μm shoulder in H_2O would be outside the observation range for D_2O.) The case for the 1.4 μm peak in D_2O, however, largely depends on the accuracy of the Gaussian approximation for the spectrum of thermalized electron in the near-infrared.

4.2. "Slow Regime" (t > 1 ps). To better characterize the slow regime (in which E_{max} is locked, within the accuracy of our measurement, near its equilibrium value and the line width continues to change), the experimental TA spectra shown in Figures 4b and 5b were fit to the same Lorentzian−Gaussian curves used to simulate the spectrum of hydrated electron:[26,37,38]

$$S(E) = (1 + [(E - E_{max})/W_L]^{\nu})^{-1} \quad \text{for } E > E_{max} \quad (2)$$

$$S(E) = \exp(-[(E - E_{max})/W_G]^2) \quad \text{for } E < E_{max} \quad (3)$$

where E is the photon energy (the spectrum $S(E)$ is normalized at the band maximum at $E = E_{max}$), $\nu = 2$ is the exponent, and W_L and W_G are the Lorentzian and Gaussian widths, respectively. Each spectrum $S(E,t)$ averaged over the $(t_1, t_1 + \Delta t)$ window has been fitted to eqs 2 and 3 using least-squares optimization (with a floating scaling factor), and the optimum parameters E_{max}, W_L, and W_G are plotted in Figure 8 vs the delay time t_1 ($\Delta t = 30$ fs slices).

It is obvious from these plots that the increase in the band energy E_{max} is much faster than the decrease in W_G (compare Figure 8a,b). For t > 0.5 ps, both of these parameters exponentially approach their respective equilibrium values E^{∞}_{max} and W^{∞}_G. For E_{max}, the corresponding first-order rate constant is ca. 3.1 ps^{-1} (which compares well with other estimates; see, e.g., refs 3−9, 16, and 17). For W_G, the rate constants are 1.62 ± 0.4 ps^{-1} for H_2O and 1.45 ± 0.2 ps^{-1} for D_2O. It is this large difference in the corresponding rate constants that accounts for the occurrence of the slow regime discussed above: for t > 1−1.2 ps, E_{max} is already very close to E^{∞}_{max} (<20 meV), whereas W_G still changes, being 50−100 meV greater than W^{∞}_G. On the basis of this observation, one can globally fit the time evolution for the entire red wing of the electron spectrum $S(E,t)$ for t > 1 ps using eq 3 with $E_{max}(t) = E^{\infty}_{max}$ and

$$W_G(t) = W^{\infty}_G + (W^{max}_G - W^{\infty}_G)\exp(-t/\tau_G) \quad (4)$$

where W^{max}_G is the Gaussian width extrapolated to $t = 0$ and τ_G is the time constant of the spectral narrowing. In Figures 9 and 6S least-squares fits to the $S(E,t)$ kinetics for electron in light and heavy water, respectively, are shown for traces obtained between 0.85 and 1.3 μm. As seen from these plots, despite having only two adjustable parameters, W^{max}_G and τ_G, eqs 3 and 4 give remarkably good approximation to these traces. The following estimates were obtained for these two parameters (95% confidence limits): $W^{max}_G = 1.18 \pm 0.04$ eV and $\tau_G = 0.56 \pm 0.01$ ps (for H_2O) and $W^{max}_G = 1.2 \pm 0.03$ eV and $\tau_G = 0.64 \pm 0.01$ ps (for D_2O). Thus, in agreement with the analysis given in Figure 8b, the spectral narrowing in D_2O is slower than in H_2O, by ca. 15 ± 5%.

Figure 8c shows the evolution of W_L of the absorption line as a function of the delay time t_1. After the first 1 ps following the photoionization, this width slowly increases from 0.4 to 0.5 eV, in approximately the same fashion for light and heavy water. When the integral under the spectrum profile is plotted vs the delay time (Figure 8d), it is almost constant with time (±10%), suggesting that in the slow regime, the oscillator strength of the transition does not change with time: the narrowing on the red side is compensated for by the broadening on the blue side. (However, it is difficult to establish this constancy accurately because the TA spectrum on the blue side is followed to λ = 0.4 μm only.)

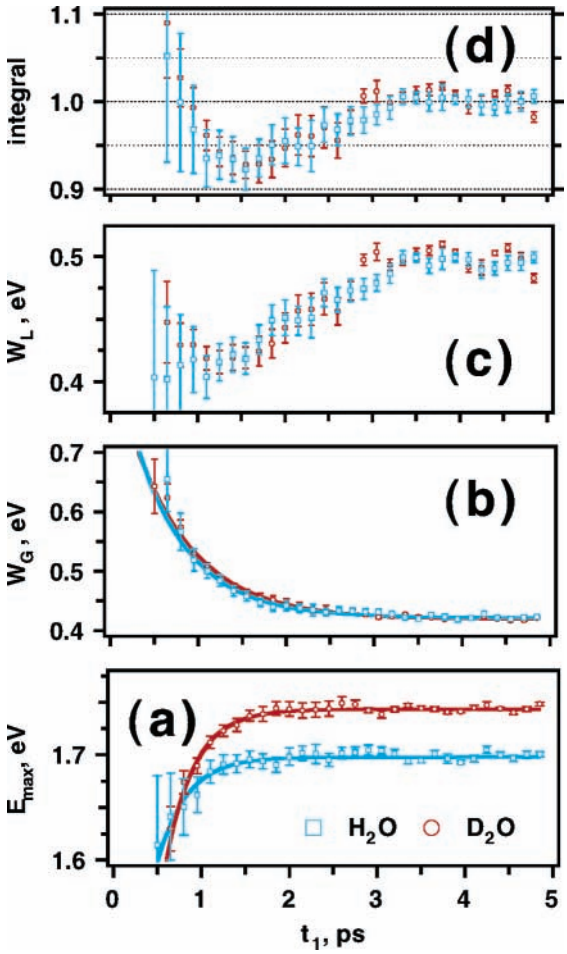

Figure 8. Gaussian−Lorentzian analysis of linearly interpolated $S(\lambda,t)$ data for the electron in light (open squares) and heavy (open circles) water. Vertical bars are 95% confidence limits determined by least-squares optimization. The solid lines in a and b are exponential fits. (a) The position of the spectrum maximum, (b) Gaussian width, (c) Lorentzian width, and (d) the integral under the spectrum plotted as a function of the delay time t_1 for $\Delta t = 30$ fs.

The slow regime identified in the present study has actually been observed previously, by Pépin et al.[6] These workers carried out a Gaussian−Lorentzian analysis similar to that outlined above for the electron generated by multiphoton ionization of liquid D_2O ($\lambda = 0.5-1.4$ μm). As seen from Figures 3 and 4 in ref 6, the Gaussian width systematically decreased with delay time, much like the same quantity in Figure 8b. To account for this apparent contradiction with the continuous shift model, Pépin et al.[6] postulated that the spectrum of the electron slides over a "supplementary component" from an unknown species having a lifetime of 2 ps that absorbs at 0.8−1.2 μm (see Figure 8 therein). Subsequently, these observations were reinterpreted in terms of a "hybrid" model[23,24] in which two species, the wet electron and the solvated electron, both undergo continuous blue shift on the sub-picosecond time scale; concurrently, the wet

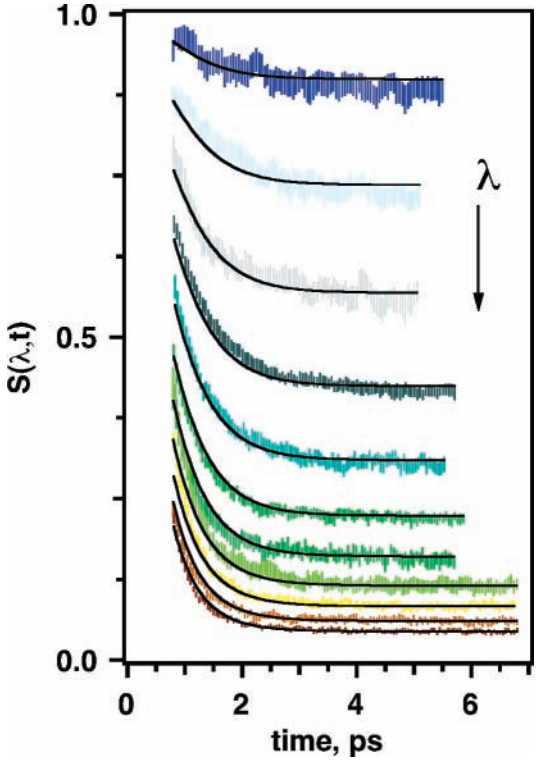

Figure 9. "Global" least-squares analysis of $S(\lambda,t)$ kinetics using the spectrum-narrowing model (eqs 3 and 4) for the electron in light water. The solid lines are simulated kinetics for, from top to bottom, $\lambda = 0.8$, 0.85, 0.9, 0.95, 1, 1.05, 1.1, 1.2, 1.25, and 1.3 μm. The vertical bars are 95% confidence limits.

electron converts to the solvated electron. Analogies to the electron solvation in alcohols[25] were drawn to substantiate this model.

The hybrid model, much like the original continuous shift model, assumes that the spectral profile of the electron(s) does not change during the relaxation of the solvent (when the spectrum shifts) or, at the very least, this profile is a Gaussian−Lorentzian function. No justification has been given for either one of these two basic assumptions, and the hybrid model has as much fidelity as the supplementary component model suggested in ref 6. Naturally, such elaborate models are nearly impossible to falsify because arbitrary properties can be postulated for hypothetical progenitors of various spectral components. We believe that it would be more appropriate to interpret these observations at their face value, i.e., as evidence that the spectral profile of the ground-state electron does evolve with time and, at short delay times, deviates strongly from the Gaussian−Lorentzian form. As demonstrated above, the entire set of TA kinetics for the electron in H_2O and D_2O in the near-infrared can be fit using the simplest spectrum-narrowing model with only two adjustable parameters.

Another concern is whether our observations can be explained using the thermal jump model of Madsen et al.[15] or the cavity contraction model of Unterreiner and co-workers.[13] The answer is negative, because, in their predictions, these two (seemingly different) models are almost indistinguishable from the continuous shift model. Within the framework of these models, the change in E_{max} is interpreted either in terms of the decrease in the temperature of the water shell around the electron[15] or the mean square dispersion of its position with respect to the cavity center.[13] As for the latter model, the shape stability is the implicit assumption, i.e., the cavity contraction model is a reformulation of the continuous shift model. The temperature jump model, despite its different physical context, is also a variant of the continuous shift model: Since the width of the e_{aq}^- spectrum changes with increasing temperature much slower than does E_{max} (see Appendix A), simulations using this model yield spectral evolution which is very similar to that given by the continuous shift model. Furthermore, even a cursory analysis of the data in Figure 8a,b points to a major inconsistency: while a temperature shift of 30 K would suffice to account for the position of the band maximum at $t = 0.5$ ps, a temperature shift of 200 K would be needed to account for the width of the electron spectrum (see Figure 1Sb). This conclusion, however, refers to the parametrization of the e_{aq}^- spectra vs temperature used by Madsen et al.,[15] and this parametrization is not supported by more recent studies. In particular, Bartels et al.[37,38] observed substantial deviations of the spectral profile of hydrated electron in hot water from the Gaussian−Lorentzian curve given by eqs 3 and 4 with the temperature-independent parameter $\upsilon = 2$. They demonstrated that, in hot water, the spectral profile is given by a modified eq 3 with υ that increases with the temperature and a temperature-independent width W_L. The resulting "hot-water" spectra become increasingly flatter at the top at higher temperature.[37,38] Given these recent developments, we reanalyzed the $S(\lambda,t)$ set in the spirit of the temperature jump model, using modified eq 3 for constant W_L and time-dependent parameters E_{max} , W_G, and υ (see Appendices A.1 and A.3). As shown therein, the temperature jump model is not supported by our results, no matter which parametrization of the e_{aq}^- spectrum is used.

The spectral narrowing described by eq 3 complemented by eq 4 (Figures 9 and 6S) naturally accounts for the major trend shown in Figures 1−3: the greater is the difference $E_{max}^{\infty} - E$ (>0) for a given photon energy E, the faster is the decay of the electron absorbance at the corresponding wavelength. By increasing the bulk temperature or by addition of salt, it is possible to, respectively, red- or blue-shift the spectrum of hydrated electron (i.e., to decrease or increase E_{max}^{∞}).[39,40] Since the initial spectrum of presolvated electron does not change significantly as a function of temperature or salinity, the basic prediction of the spectrum-narrowing model (assuming weak temperature dependence for the relaxation time τ_G in eq 4) is that, for a fixed probe wavelength on the red side of the e_{aq}^- spectrum, the decay of the absorption is progressively slower with increasing temperature and progressively faster with increasing salinity. Both of these trends are consistent with the experimental observations of Unterreiner and co-workers[13] and Crowell and co-workers[33,41] (for the temperature effect) and Sauer et al.[39] (for the salinity effect).

4.3. Spectral Evolution: Possible Mechanisms. From the theoretical perspective, the chief appeal of the "continuous shift" model is a possibility to reduce the complex spectral evolution of the electron to a single time-dependent parameter $E_{max}(t)$ related to the average electron energy; the latter quantity may be obtained directly from mixed quantum-classical molecular dynamics (MD) simulations in which the excess electron is treated quantum-mechanically, whereas the solvent molecules are treated classically.[42−49] If the continuous shift model were incorrect, such a simplified approach would be insufficient: time-resolved spectra of the electron should be simulated instead.[44,45] The latter is a more complicated problem[44−47] which requires the detailed knowledge of the ground and excited states, transition probabilities, etc. Even for fully hydrated, thermally relaxed electron, the origin of the basic features in its absorption spectrum is the subject of ongoing controversy and continuing

research, despite the decades of modeling at all levels of theory, including, most recently, Car−Parrinello density functional MD modeling.[51]

The current consensus is that the bell-shaped band centered at 720 nm is from three partially merged s → p subbands; these subbands correspond to the three orientations of the p orbital with respect to the principal axes of the ellipsoidal solvation cavity.[43−45] While this simple picture is supported by MD[42−49] and other[51] calculations, hole burning absorption anisotropy experiments by Assel et al.[11] and, more recently, Cavanagh et al.[12] did not yield the anticipated polarization-dependent TA dynamics. Some anisotropy was observed in the experiments of Reid et al.;[52] however, even in that study the depolarization dynamics were quite different from the theoretical predictions of Schwartz and Rossky.[45] A possible rationale for these discrepancies was proposed by Bratos and Leicknam[50] who postulated rapid (<10 fs) internal relaxation in the p-state manifold following the photoexcitation of the s-state hydrated electron. Importantly, the rapid decay of the photon echo following the s → p photoexcitation observed by Wiersma and co-workers[10] cannot be considered as unequivocal evidence for fast dephasing in the p-state manifold since a rapid Stokes shift can also qualitatively account for their results.[49]

While a clear-cut demonstration of the substructure in the electron spectrum by means of ultrafast spectroscopy is lacking, indirect support for the p-state nondegeneracy is given by resonance Raman spectra of e_{aq}^-:[53−55] Tauber and Mathies[54] determined the depolarization ratio across the entire Raman spectrum of e_{aq}^- in liquid H_2O and concluded that this ratio (ca. 0.3−0.5) is incompatible with a resonant transition to a *single* nondegenerate state. Their analyses suggest that homogeneous broadening for e_{aq}^- is at least 100 times greater than inhomogeneous broadening[53a,54] and the width of the s → p band on the red side is determined by vibrational progressions from the five strongest modes with wavenumbers between 470 and 3100 cm^{-1} (for H_2O).[53a] Thus, it appears that a full quantum mechanical treatment of water vibrations is needed to rationalize the shape of the absorption spectrum.

It is apparent from these results that the absorption profile is controlled by many factors, and only advanced theory can account both for the spectrum of hydrated electron and the spectral evolution of its precursor in the course of solvation. As stated in the Introduction, given the previous record of kinetic modeling, we do not feel compelled to provide yet another many-species reaction scheme "explaining" the solvation dynamics. Only a comprehensive, rigorous theory would be up to this task. Still, it is appropriate to speculate on the origin of the novel features reported in this study, namely, (i) the spectral narrowing/broadening that occurs in the slow regime (for $t > 1$ ps) and (ii) the differences between the TA spectra for the excess electron in H_2O and D_2O (observed for $t < 1$ ps).

The characteristic spectral transformations observed in the slow regime, viz., the narrowing of the band on the red side and broadening on the blue side, bear qualitative resemblance to the evolution of the absorption bands from electronically excited molecules undergoing vibrational relaxation. Such a relaxation involves nonequilibrium populations of vibrational states which according to Tauber and Mathies[53,54] determine the shape and the width of the red side of the e_{aq}^- spectrum. This vibrational relaxation readily explains the isotope dependence for the time constant of spectral narrowing. The time scale for the vibration relaxation in liquid water (ca. 0.75−1 ps for the O−H stretch in the room-temperature HOD:D_2O)[56,57] compares well with the observed time scale of spectrum narrowing in our experiment.

Another possible rationale is a time-dependent change in the relative positions and the weights of the p subbands, although the origin of the isotope effect is less clear in such a case. If the p subbands do define the shape of the electron spectrum in the visible and near-infrared, as suggested by numerous MD calculations, the slow regime may be interpreted as gradual increase in the sphericity of the solvation cavity during its relaxation. That, in turn, suggests that the initial localization of the electron involves a contorted, highly anisotropic trap. Such an assertion is in agreement with the theoretical models of electron localization in liquid water.[30] Indirect experimental support for this assertion is provided by the data on electron trapping in hexagonal ice: quasifree electrons were shown[19,59] to localize on (highly anisotropic) Bjerrum defects;[60] after this initial localization, the water structure around such a defect relaxes and a near-spherical solvation cavity gradually emerges on a picosecond time scale.[61] The resulting spectrum bears strong resemblance to the spectrum of hydrated electron and changes little between 4 and 270 K.[19,20]

It seems likely to these authors that the changing sphericity of the solvation cavity is the ultimate cause for the failure of the continuous shift and temperature jump models to capture the essentials of the spectral evolution on the sub-picosecond time scale. In these models, the environment of the electron during its solvation is assumed to have the same degree of isotropy as fully relaxed, hydrated electron, either at the final or elevated temperature. Perhaps the increase in the sphericity of the solvation cavity (both on sub-picosecond time scale and at later delay times) occurs in concert with the vibrational relaxation of solvent molecules forming the solvation cavity (see above); such a concerted mechanism would account for the isotope effect on the spectral narrowing.

On the sub-picosecond time scale, the vibrations in water appear to have a strong effect on the spectral evolution. Indeed, new spectral features were observed in the near-infrared, where the water molecules have O−H and O−D stretch overtones. As explained in section 4.2, the thermal effect (a photoinduced change in the refraction index of water) does not appear to cause these features. Still, the vibrations of water molecules are implicated. Due to the observed isotope selectivity, many potential candidates for the progenitors of these features, for instance, the IR-absorbing p-state electron examined theoretically by Schwartz and Rossky[45] and experimentally by Barbara and co-workers[7,9,52] and others,[11,12] can be excluded since the generation of such a species in the course of photoionization, while plausible, does not account for these specific features. We stress that our data (as well as the previous studies; see Kambhampati et al.[9] for more discussion) do not provide clear-cut evidence either against or for such an involvement, on a very short time scale (<300 fs). The same refers to the involvement of the tentative wet electron[6,11,16,22−25] and liquid-water analogue of the IR-absorbing electron in low-temperature ice[19−21] postulated by others.

We believe that the 1.15 and 1.3−1.4 μm features for the excess electron in H_2O emerge due to collective excitation of the electronic and vibrational modes of the presolvated electron by the probe light, when the corresponding energies are close. It is possible that the same features are present in the TA spectra of s → p excited hydrated electrons.[7−9,11] Recently, Thaller et al.[58] obtained the first near- and mid-infrared TA spectra of photoexcited hydrated electrons (to 5 μm). Unfortunately, the quality of these TA spectra is insufficient to decide whether

the fine features observed in this study are present (see Figures 2 and 3 in ref 58). However, the studies of Thaller et al.[58] and Laenen et al.[16] indicate that the electronic and vibrational degrees of freedom are strongly coupled in the precursor(s) of the hydrated electron, as suggested by its short-lived (<200 fs) diffuse absorption band (1−5 μm) increasing toward the location of the O−H stretch in water. In the photon echo and transient grating experiments of Wiersma and co-workers, a librational motion of water molecules (ca. 850 cm^{-1}) in the relaxation dynamics of electrons following s → p photoexcitation was observed. Resonance Raman spectra of the hydrated electron indicate strong coupling of the s → p electronic transition to the O−H stretch and bend modes.[53−55] Such a coupling would be expected on the theoretical grounds since the O−H groups with protons pointing out toward the cavity center comprise the core of the solvated electron.[42−47] Vibronic transitions in the near-infrared would be another manifestation of this strong coupling. Specifically, we suggest that O−H vibrations can be excited when the energy of the electronic transition for presolvated electron (or a subset of such electrons) is close to that of the O−H stretch overtone. To our knowledge, such a possibility has not been addressed theoretically, while it might be suggested by the results of the present work. In the currently popular mixed quantum-classical MD[43−47] and path integral[42] models of excess electrons in liquids, the solvent is treated classically and such phenomena as vibronic coupling and vibrational relaxation for hydrated electron cannot be addressed. The results discussed above suggest that these phenomena might play important roles in the electron solvation dynamics; hence, more advanced models might be needed.

5. Conclusion

The evolution of the TA spectra in the visible and near-infrared, for the presolvated electron, following biphotonic excitation of room-temperature light and heavy water, has been studied. Two regimes of the spectral evolution were observed. In both of these regimes, the spectral profile changes with delay time; the continuous blue shift,[6,22] temperature jump,[15] and cavity contraction[13] models that assume the constancy or near-constancy of this spectral profile (as the electron spectrum shifts to the blue) are not supported by our data. On the sub-picosecond time scale, the band maximum systematically shifts to higher photon energy and the spectrum narrows (Figures 4a, 5a, and 5S). At later delay times (>1 ps), the position of the band maximum is "locked" within 20 meV of its equilibrium value, but the spectral profile continues to change, by narrowing on the red side and broadening on the blue side (Figures 4b and 5b). The oscillator strength of the transition is constant within 10% during this relatively slow, small-scale spectral transformation. The spectral narrowing can be accounted for by a two-parameter model in which the width of the Gaussian half-line exponentially decreases with the delay time. The time constant of this narrowing is ca. 0.56 ps for H_2O and 0.64 ps for D_2O, respectively.

In the first picosecond after photoionization, two new features (the 1.15 μm band and 1.4 μm shoulder) were observed in the near-infrared spectra for the electron in H_2O; the 1.4 μm feature observed for electron in D_2O is likely to be an analogue of the 1.15 μm feature in H_2O. These features are observed in the same region where O−H and O−D overtones appear in the spectrum of liquid water. While it cannot be entirely excluded that these features are artifacts of the data analysis, it seems more likely that these bands are genuine and originate through the vibronic transitions of presolvated electron, or a subset of such electrons. The isotope-dependent narrowing/broadening of the absorption band of the electron for $t > 1$ ps can be interpreted as evidence for the occurrence of vibrational relaxation in the water molecules lining the solvation cavity. In both of these regimes, continuous decrease in the size and increase in the sphericity of the solvation cavity causes a time-dependent blue shift and decrease in the splitting between the three p subbands of the electron. These two trends would qualitatively account for the observed spectral evolution.

Since the current MD theories of hydrated electron[42−49] do not include the quantum degrees of freedom for vibrations in water molecules, the vibrational relaxation and the vibronic coupling hinted at by our results presently cannot be modeled. While there are models which treat the vibrations quantum-mechanically, albeit in a greatly simplified fashion,[57,62] these models cannot address the solvation dynamics. Further development of the theory would be necessary for a self-consistent explanation of the spectral evolution during the solvation and thermalization of the electron in liquid water.

Acknowledgment. We thank Profs. B. J. Schwartz and P. F. Barbara and Drs. S. Pommeret, C. D. Jonah, and D. M. Bartels for many useful discussions. We thank Dr. D. M. Bartels for the permission to reproduce his unpublished data. The research at the ANL was supported by the Office of Science, Division of Chemical Sciences, U.S. Department of Energy, under Contract No. W-31-109-ENG-38.

Supporting Information Available: (1, pdf) (a) Appendix A, absorption spectrum of hydrated electron, (b) Appendix B, instruction for the retrieval of kinetic data from the supplied ASCII file, and (c) Figures 1S−7S with captions and (2, txt) 288 Kb ASCII file named "H2O_D2O_traces.txt" containing digitized kinetic traces $S(\lambda,t)$ for the electron in H_2O and D_2O. This material is available free of charge via the Internet at http://pubs.acs.org.

References and Notes

(1) Migus, A.; Gauduel, Y.; Martin, J. L.; Antonetti, A. *Phys. Rev. Lett.* **1987**, *58*, 1559.

(2) Long, F. H.; Lu, H.; Eisenthal, K. B. *Chem. Phys. Lett.* **1989**, *160*, 464; *J. Chem. Phys.* **1989**, *91*, 4413. Lu, H.; Long, F. H.; Bowman, R. M.; Eisenthal, K. B. *J. Phys. Chem.* **1989**, *93*, 27. Long, F. H.; Lu, H.; Eisenthal, K. B. *Phys. Rev. Lett.* **1990**, *64*, 1469. Long, F. H.; Lu, H.; Shi, X.; Eisenthal, K. B. *Chem. Phys. Lett.* **1990**, *169*, 165; *Chem. Phys. Lett.* **1991**, *185*, 47.

(3) Gauduel, Y.; Pommeret, S.; Migus, A.; Antonetti, A. *J. Phys. Chem.* **1989**, *93*, 3880; *Chem. Phys.* **1990**, *149*, 1; *J. Phys. Chem.* **1991**, *95*, 533. Pommeret, S.; Antonetti, A.; Gauduel, Y. *J. Am. Chem. Soc.* **1991**, *113*, 9105. Gauduel, Y.; Pommeret, S.; Antonetti, A. *J. Phys. Chem.* **1993**, *97*, 134. See also: Goulet, T.; Jay-Gerin, J.-P. *J. Phys. Chem.* **1989**, *93*, 7533.

(4) Gauduel, Y.; Pommeret, S.; Yamada, N.; Migus, A.; Antonetti, A. *J. Am. Chem. Soc.* **1989**, *111*, 4974.

(5) Gauduel, Y. In *Ultrafast Dynamics of Chemical Systems*; Simon, J. D., Ed.; Kluwer: Amsterdam, 1994; p 81.

(6) Pepin, C.; Goulet, T.; Houde, D.; Jay-Gerin, J.-P. *J. Phys. Chem. A* **1997**, *101*, 4351. The photophysics of multiphoton water ionization pertinent for this study is discussed in: Pepin, C.; Houde, D.; Remita, H.; Goulet, T.; Jay-Gerin, J.-P. *Phys. Rev. Lett.* **1992**, *69*, 3389.

(7) Alfano, J. C.; Walhout, P. K.; Kimura, Y.; Barbara, P. F. *J. Chem. Phys.* **1993**, *98*, 5996. Kimura, Y.; Alfano, J. C.; Walhout, P. K.; Barbara, P. F. *J. Phys. Chem.* **1994**, *98*, 3450. Silva, C.; Walhout, P. K.; Yokoyama, K.; Barbara, P. F. *Phys. Rev. Lett.* **1998**, *80*, 1086. Yokoyama, K.; Silva, C.; Son, D.-H.; Walhout, P. K.; Barbara, P. F. *J. Phys. Chem. A* **1998**, *102*, 6957.

(8) Kee, T. W.; Son, D.-H.; Kambhampati, P.; Barbara, P. F. *J. Phys. Chem. A* **2001**, *105*, 8434. Son, D.-H.; Kambhampati, P.; Kee, T. W.; Barbara, P. F. *Chem. Phys. Lett.* **2001**, *342*, 571. Son, D.-H.; Kambhampati, P.; Kee, T. W.; Barbara, P. F. *J. Phys. Chem. A* **2001**, *105*, 8269.

(9) Kambhampati, P.; Son, D.-H.; Kee, T. W.; Barbara, P. F. *J. Phys. Chem. A* **2002**, *106*, 2374.

(10) Emde, M. F.; Baltuska, A.; Kummrow, A.; Pshenichnikov, M. S.; Wiersma, D. A. *Phys. Rev. Lett.* **1998**, *80*, 4645. Kummrow, A.; Emde, M.

F.; Baltuska, A.; Pshenichnikov, M. S.; Wiersma, D. A. *J. Phys. Chem. A* **1998**, *102*, 4172; *Z. Phys. Chem.* **1999**, *212*, 153. Pshenichnikov, M. S.; Baltuska, A.; Wiersma, D. A. *Chem. Phys. Lett.* **2004**, *389*, 171.

(11) Assel, M.; Laenen, R.; Laubereau, A. *J. Phys. Chem. A* **1998**, *102*, 2256; *J. Chem. Phys.* **1999**, *111*, 6869.

(12) Cavanagh, M. C.; Martini, I. B.; Schwartz, B. *J. Chem. Phys. Lett.* **2004**, *396*, 359.

(13) Hertwig, A.; Hippler, H.; Unterreiner, A. N.; Voehringer, P. *Ber. Bunsen-Ges. Phys. Chem.* **1998**, *102*, 805; *Phys. Chem. Chem. Phys.* **1999**, *1*, 5663; *J. Phys.: Condens. Matter* **2000**, *12*, A165; *Phys. Chem. Chem. Phys.* **2002**, *2002*, 4412.

(14) Thomsen, C. L.; Madsen, D.; Keiding, S. R.; Thoegersen, J.; Christiansen, O. *J. Chem. Phys.* **1999**, *110*, 3453.

(15) Madsen, D.; Thomsen, C. L.; Thoegersen, J.; Keiding, S. R. *J. Chem. Phys.* **2000**, *113*, 1126.

(16) Laenen, R.; Roth, T.; Laubereau, A. *Phys. Rev. Lett.* **2000**, *85*, 50. Laenen, R.; Roth, T. *J. Mol. Struct.* **2001**, *598*, 37.

(17) Vilchiz, V. H.; Kloepfer, J. A.; Germaine, A. C.; Lenchenkov, V. A.; Bradforth, S. E. *J. Phys. Chem. A* **2001**, *105*, 1711.

(18) Bovensiepen, U.; Gahl, C.; Wolf, M. *J. Phys. Chem. B* **2003**, *107*, 8706. Gahl, C.; Bovensiepen, U.; Frischkorn, C.; Morgenstern, K.; Reider, K.-H.; Wolf, M. *Surf. Sci.* **2003**, *532*−*535*, 108. Gahl, C.; Bovensiepen, U.; Frischkorn, C.; Wolf, M. *Phys. Rev. Lett.* **2002**, *89*, 107402.

(19) Gillis, H. A.; Quickenden, T. A. *Can. J. Chem.* **2001**, *79*, 80. Kroh, J. In *Pulse Radiolysis*; Tabata, Y., Ed.; CRC Press: Roca Baton, FL, 1990; p 357.

(20) Buxton, G. B.; Gillis, H. A.; Klassen, N. V. *Can. J. Chem.* **1977**, *55*, 2385. Buxton, G. B.; Gillis, H. A.; Teather, G. G.; Ross, C. K. *J. Phys. Chem.* **1980**, *84*, 1248. Trudel, G. J.; Gillis, H. A.; Klassen, N. V.; Teather, G. G. *Can. J. Chem.* **1981**, *59*, 1235. Kawabata, K.; Nagata, Y.; Okabe, S.; Kimura, N.; Tsumori, K.; Kawanishi, M.; Buxton, G. B.; Salmon, G. A. *J. Chem. Phys.* **1982**, *77*, 3884. Wu, Z.; Gillis, H. A.; Klassen, N. V.; Teather, G. G. *J. Chem. Phys.* **1983**, *78*, 2449. Muto, H.; Matsuura, K.; Nunome, K. *J. Phys. Chem.* **1992**, *96*, 5211.

(21) Nilsson, G. *J. Chem. Phys.* **1972**, *56*, 3427.

(22) Keszei, E.; Murphrey, T. H.; Rossky, P. J. *J. Phys. Chem.* **1995**, *99*, 22.

(23) Jay-Gerin, J.-P. *Can. J. Chem.* **1997**, *75*, 1310.

(24) Goulet, T.; Pepin, C.; Houde, D.; Jay-Gerin, J.-P. *Radiat. Phys. Chem.* **1999**, *54*, 441.

(25) Pepin, C.; Goulet, T.; Houde, D.; Jay-Gerin, J.-P. *J. Phys. Chem.* **1994**, *98*, 7009.

(26) Jou, F.-Y.; Freeman, G. R. *J. Phys. Chem.* **1979**, *83*, 2383.

(27) Crowell, R. A.; Bartels, D. M. *J. Phys. Chem.* **1996**, *100*, 17713. Bartels, D. M.; Crowell, R. A. *J. Phys. Chem. A* **2000**, *104*, 3349.

(28) Sander, M. U.; Luther, K.; Troe, J. *Ber. Bunsen-Ges. Phys. Chem.* **1993**, *97*, 953; *J. Phys. Chem.* **1993**, *97*, 11489. Sander, M. U.; Gudiksen, M. S.; Luther, K.; Troe, J. *Chem. Phys.* **2000**, *258*, 257.

(29) Lian, R.; Oulianov, D. A.; Shkrob, I. A.; Crowell, R. A. *Chem. Phys. Lett.* **2004**, *398*, 102.

(30) Tachiya, M.; Mozumder, A. *J. Chem. Phys.* **1974**, *60*, 3037; *J. Chem. Phys.* **1974**, *61*, 3890.

(31) Bartczak, W. M.; Kroh, J. *Chem. Phys.* **1979**, *44*, 251. Bartczak, W. M.; Sopek, M.; Kroh, J. *Radiat. Phys. Chem.* **1989**, *34*, 93. Bartczak, W. M.; Pernal, K. *Res. Chem. Intermed.* **2001**, *27*, 891. Hilczer, M.; Bartczak, W. M.; Sopek, M. *J. Chem. Phys.* **1986**, *85*, 6813. Hilczer, M.; Bartczak, W. M.; Kroh, J. *J. Chem. Phys.* **1988**, *89*, 2286. Hilczer, M.; Bartczak, W. M. *Radiat. Phys. Chem.* **1992**, *39*, 85.

(32) Houee-Levin, C.; Tannous, C.; Jay-Gerin, J.-P. *J. Phys. Chem.* **1989**, *93*, 7074. Goulet, T.; Bernas, A.; Ferradini, C.; Jay-Gerin, J.-P. *Chem. Phys. Lett.* **1990**, *170*, 492. Bernas, A.; Ferradini, C.; Jay-Gerin, J.-P. *Chem. Phys.* **1997**, *222*, 151.

(33) Lian, R.; Crowell, R. A.; Shkrob, I. A.; Bartels, D. M.; Chen, X.; Bradforth, S. E. *J. Chem. Phys.* **2004**, *120*, 11712.

(34) Shkrob I. A.; Crowell, R. *Phys. Rev. B.* **1998**, *57*, 12207, and references therein.

(35) Fauchet, P. M.; Hulin, D.; Vanderhaghen, R.; Mourchid, A.; Nighan, W. L., Jr. *J. Non-Cryst. Solids* **1992**, *141*, 76, and references therein.

(36) Sauer, M. C., Jr.; Crowell, R. A.; Shkrob, I. A. *J. Phys. Chem. A* **2004**, *108*, 5490. Bartels, D. M.; Crowell, R. A. *J. Phys. Chem. A* **2000**, *104*, 3349.

(37) Bartels, D. M.; Takahashi, K.; Cline, J. A.; Marin, T. W.; Jonah, C. D. *J. Phys. Chem. A*, **2005**, *109*, 1299.

(38) Bartels, D. M. Private communication.

(39) Sauer, M. C., Jr.; Shkrob, I. A.; Lian, R.; Crowell, R. A.; Bartels, D. M.; Chen, X.; Suffern, S.; Bradforth S. E. *J. Phys. Chem. A* **2004**, *108*, 10414.

(40) Hart, E. J.; Anbar, M. *The Hydrated Electron*; Wiley-Interscience: New York, 1970. Anbar, M.; Hart, E. J. *J. Phys. Chem.* **1965**, *69*, 1244.

(41) Crowell, R. A.; Lian, R.; Shkrob, I. A.; Qian, Jun; Oulianov, D. A.; Pommeret, S. *J. Phys. Chem. A* **2004**, *108*, 9105.

(42) Schnitker, J.; Rossky, P. J. *J. Chem. Phys.* **1986**, *86*, 3471. Wallqvist, A.; Thirumalai, D.; Berne, B. J. *J. Chem. Phys.* **1986**, *86*, 6404. Romero, C.; Jonah, C. D. *J. Chem. Phys.* **1988**, *90*, 1877. Wallqvist, A.; Martyna, G.; Berne, B. J. *J. Phys. Chem.* **1988**, *92*, 1721. Miura, S.; Hirata, F. *J. Phys. Chem.* **1994**, *98*, 9649.

(43) Schnitker, J.; Rossky, P. J.; Kenney-Wallace, G. A. *J. Chem. Phys.* **1986**, *85*, 1986. Rossky, P. J.; Schnitker, J. *J. Phys. Chem.* **1988**, *92*, 4277. Schnitker, J.; Motakabbir, K.; Rossky, P. J.; Friesner, R. A. *Phys. Rev. Lett.* **1988**, *60*, 456. Webster, F. J.; Schnitker, J.; Frierichs, M. S.; Friesner, R. A.; Rossky, P. J. *Phys. Rev. Lett.* **1991**, *66*, 3172. Webster, F. J.; Rossky, P. J.; Friesner, R. A. *Comput. Phys. Commun.* **1991**, *63*, 494. Motakabbir, K.; Schnitker, J.; Rossky, P. J. *J. Chem. Phys.* **1992**, *97*, 2055.

(44) Murphrey, T. H.; Rossky, P. J. *J. Chem. Phys.* **1993**, *99*, 515.

(45) Schwartz, B. J.; Rossky, P. J. *J. Chem. Phys.* **1994**, *101*, 6917; *J. Phys. Chem.* **1994**, *98*, 4489; *Phys. Rev. Lett.* **1994**, *72*, 3282; *J. Chem. Phys.* **1994**, *101*, 6902.

(46) Wong, K. F.; Rossky, P. J. *J. Phys. Chem. A* **2001**, *105*, 2546.

(47) Borgis, D.; Staib, A. *Chem. Phys. Lett.* **1994**, *230*, 405. Staib, A.; Borgis, D. *J. Chem. Phys.* **1995**, *1995*, 2642. Borgis, D.; Staib, A. *J. Chim. Phys.* **1996**, *39*, 1628; *J. Chem. Phys.* **1996**, *104*, 4776; *J. Phys.: Condens. Matter* **1996**, *8*, 9389. Staib, A.; Borgis, D. *J. Chem. Phys.* **1996**, *104*, 9027. Borgis, D.; Bratos, S. *J. Mol. Struct.* **1997**, *1997*, 537.

(48) Nicolas, C.; Boutin, A.; Levy, B.; Borgis, D. *J. Chem. Phys.* **2003**, *118*, 9689.

(49) Rosenthal, S. J.; Schwartz, B. J.; Rossky, P. J. *Chem. Phys. Lett.* **1994**, *229*, 443.

(50) Bratos, S.; Leicknam, J.-C. *J. Chem. Phys.* **1998**, *109*, 9950. Bratos, S.; Leicknam, J.-C.; Borgis, D.; Staib, A. *Phys. Rev. E* **1997**, *55*, 7217.

(51) Boero, M.; Parrinello, M.; Terakura, K.; Ikeshoji, T.; Liew, C. C. *Phys. Rev. Lett.* **2003**, *90*, 226403.

(52) Reid, P. J.; Silva, C.; Wallhout, P. K.; Barbara, P. F. *Chem. Phys. Lett.* **1994**, *228*, 658.

(53) (a) Tauber, M. J.; Mathies, R. A. *Chem. Phys. Lett.* **2002**, *354*, 518. (b) Tauber, M. J.; Mathies, R. A. *J. Phys. Chem. A* **2001**, *105*, 10952.

(54) Tauber, M. J.; Mathies, R. A. *J. Am. Chem. Soc.* **2003**, *125*, 1394.

(55) Mizuno, M.; Tahara, T. *J. Phys. Chem. A* **2001**, *105*, 8823; *J. Phys. Chem. A* **2003**, *107*, 2411. Mizuno, M.; Yamaguchi, S.; Tahara, T. In *Femtochemistry and Femtobiology*; Martin, M. M., Hynes, J. T., Eds.; Elsevier: Amsterdam, The Netherlands, 2004; p 225.

(56) See, for example: Laubereau, A.; et al. *J. Phys. Chem. B* **2002**, *106*, 408; *J. Chem. Phys.* **1999**, *110*, 5814; *Phys. Rev. Lett.* **1998**, *80*, 2622. Dlott D. D.; et al. *J. Phys. Chem. A* **2004**, *108*, 9054; *Chem. Phys. Lett.* **2004**, *397*, 40; *Chem. Phys. Lett.* **2003**, *378*, 281; *Chem. Phys. Lett.* **2003**, *371*, 594; *J. Phys. Chem. A* **2000**, *104*, 4866. Gale, G. M.; et al. *Phys. Rev. Lett.* **1999**, *82*, 1069; *Phys. Rev. E* **2000**, *61*, 5211. Bakker, H. J.; et al. *J. Chem. Phys.* **2002**, *116*, 2592; *Science* **2002**, *297*, 587; *J. Chem. Phys.* **2002**, *117*, 1708; *J. Phys. Chem. A* **2001**, *105*, 1238; *Nature* **1999**, *402*, 507; *J. Chem. Phys.* **1999**, *111*, 1494; *Phys. Rev. Lett.* **1998**, *81*, 1106; *Phys. Rev. Lett.* **1999**, *83*, 2077; *Science* **1997**, *278*, 658. Tokmakoff, A.; et al. *Science* **2003**, *301*, 1698. Wiersma D. A.; et al. *Chem. Phys. Lett.* **2003**, *369*, 107. Elsaesser, T.; et al. *J. Phys. Chem. A* **2002**, *106*, 2341; *Phys. Rev. Lett.* **2001**, *87*, 027401. Fayer, M. D.; et al. *J. Phys. Chem. A* **2004**, *108*, 1107; *Chem. Phys. Lett.* **2004**, *386*, 295; *J. Chem. Phys.* **2004**, *121*, 8897.

(57) Rey, R.; Hynes, J. T. *J. Chem. Phys.* **1996**, *104*, 2356. Rey, R.; Møller, K. B.; Hynes, J. T. *J. Phys. Chem. A* **2002**, *106*, 11993; *Chem. Rev.* **2004**, *104*, 1915. Lawrence, C. P.; Skinner, J. L. *J. Chem. Phys.* **2002**, *117*, 5827 and 8848; *J. Chem. Phys.* **2003**, *118*, 264 and 9664.

(58) Thaller, A.; Laenen, R.; Laubereau, A. *Chem. Phys. Lett.* **2004**, *398*, 459.

(59) Warman, J. M.; de Haas, M. P.; Verberne, J. B. *J. Phys. Chem.* **1980**, *84*, 1240. Warman, J. M.; Jonah, C. D. *Chem. Phys. Lett.* **1981**, *79*, 43. de Haas, M. P.; Kunst, M.; Warman, J. M.; Verberne, J. B. *J. Phys. Chem.* **1983**, *87*, 4089. Kunst, M.; Warman, J. M.; de Haas, M. P.; Verberne, J. B. *J. Phys. Chem.* **1983**, *87*, 4096.

(60) For MD simulations of these Bjerrum defects in *Ih* ice, see: Kobayashi, C.; Saito, S.; Ohmine, I. *J. Chem. Phys.* **2001**, *115*, 4742.

(61) Warman, J. M.; Kunst, M.; Jonah, C. D. *J. Phys. Chem.* **1983**, *87*, 4292.

(62) Mukhomorov, V. K. *Opt. Spectrosk.* **1995**, *79*, 170. Brodsky, A. M.; Tsarevsky, A. V. *J. Phys. Chem.* **1984**, *88*, 3790. Brodsky, A. M.; Vannikov, A. V.; Chubakova, T. A.; Tsarevsky, A. V. *J. Chem. Soc., Faraday Trans. 2* **1981**, *77*, 709.